Trends in Cell Biology

CellPress
REVIEWS

Review

# Investigating the Structure of Neurotoxic Protein Aggregates Inside Cells

Felix J.B. Bäuerlein [1,*], Rubén Fernández-Busnadiego [1,2,3,*] and Wolfgang Baumeister[1,*]

**Neurodegenerative diseases affect the lives of millions of people across the world, being particularly prevalent in the aging population. Despite huge research efforts, conclusive insights into the disease mechanisms are still lacking. Therefore, therapeutic strategies are limited to symptomatic treatments. A common histopathological hallmark of many neurodegenerative diseases is the presence of large pathognomonic protein aggregates, but their role in the disease pathology is unclear and subject to controversy. Here, we discuss imaging methods allowing investigation of these structures within their cellular environment: conventional electron microscopy (EM), super-resolution light microscopy (SR-LM), and cryo-electron tomography (cryo-ET). Multidisciplinary approaches are key for understanding neurodegenerative diseases and may contribute to the development of effective treatments. For simplicity, we focus on huntingtin aggregates, characteristic of Huntington's disease.**

## Highlights

Despite massive research efforts, conclusive insights into the pathomechanisms of neurodegenerative diseases are lacking.

A histopathological hallmark of neurodegenerative diseases are large protein aggregates (inclusion bodies). Their role in the disease pathology is unclear.

Methods with subcellular resolution (cryo-electron tomography, super-resolution light microscopy, and conventional electron microscopy) are invaluable to investigate the involvement of inclusion bodies in neurodegeneration.

The investigation of vital patient-derived material with those high-resolution techniques holds high potential for major breakthroughs in understanding neurodegenerative diseases and will may contribute to the development of effective treatments.

## The Role of Protein Aggregation in Neurodegeneration

Neurodegeneration is characterized by loss of function and death of neuronal cells, resulting in a progressive deterioration and loss of connectivity of neuronal circuits. These neurodegenerative processes lead to diverse syndromes like dementia, movement disorders (dystonia), and behavioral abnormalities as an expression of the so far incurable and lethal neurological diseases: Alzheimer's disease (AD), Parkinson's disease (PD), Huntington's disease (HD), amyotrophic lateral sclerosis (ALS), and other rare syndromes.

Despite massive research efforts, conclusive insights into the disease mechanisms are lacking. An enormous number of >190 000 publications (PubMed search for MeSH Terms: 'Alzheimers disease', 'Parkinsons disease', 'Huntingtons disease', and 'Amyotrophic lateral sclerosis' on 12 August 2020) is on record to date (AD: 93 000, PD: 66 000, HD: 12 000, ALS: 19 000), but a solution to the problem of neurodegeneration is not yet in sight.

A common histopathological hallmark of many neurodegenerative diseases is the presence of pathognomonic protein aggregates [1,2]. Aggregates may form due to mutations that render disease-specific proteins aggregation-prone or increase their cellular concentration. Moreover, environmental factors [3] and aging effects also play important roles. In particular, the cellular proteostasis capacity strongly declines with age [1].

Although aggregates were first identified and associated with neurodegeneration by Alois Alzheimer more than 110 years ago, their role in pathology remains controversial [4]. The term 'aggregate' should be differentiated at this point, as there are at least two distinct states: (i) small, soluble, oligomeric aggregates, which can develop into (ii) large insoluble protein aggregates known as **inclusion bodies** (**IBs**; see Glossary), reported to adopt amyloidogenic and amorphous conformations. The presence of small soluble oligomeric aggregates is strongly associated with toxicity in many of these proteinopathies, including AD [5–7], PD [8], ALS [9], and

[1]Max-Planck-Institute of Biochemistry, Department for Molecular Structural Biology, Am Klopferspitz 18, 82152 Planegg, Germany
[2]University Medical Center Göttingen, Institute for Neuropathology, Robert-Koch-Strasse 40, 37075 Göttingen, Germany
[3]Cluster of Excellence 'Multiscale Bioimaging: from Molecular Machines to Networks of Excitable Cells' (MBExC), University of Göttingen, Göttingen, Germany

*Correspondence:
baeuerlein@biochem.mpg.de (F.J.B. Bäuerlein),
ruben.fernandezbusnadiego@med.uni-goettingen.de (R. Fernández-Busnadiego),
and baumeist@biochem.mpg.de (W. Baumeister).

HD [10–17], and IB formation is often interpreted as a protective mechanism [2,18]. However, besides oligomers, IBs may also play significant cytotoxic roles in these pathologies [4], as observed for α-synuclein [8,19], Tau [20,21], TDP-43 [22,23], and amyloid beta [24]. IBs containing α-synuclein are found in PD, Lewy-body disease, multisystem atrophy, and pure autonomic failure [25]. Hyperphosphorylated tau protein precipitates cytosolically into neurofibrillary tangles found in IBs of AD, fronto-temporal dementia, progressive supranuclear palsy, and several other tauopathies [26]. TDP-43 accumulates in IBs found in ALS and fronto-temporal dementia but also in Lewy-body disease, AD, PD, HD, Pick's disease, progressive supranuclear palsy, and Guam parkinsonism–dementia complex [27]. Amyloid beta is the main constituent of the extracellular neuritic plaques found in AD and Down syndrome [28]. Although the IBs of the various neurodegenerative diseases are formed by different proteins, they typically consist of cross β-sheet amyloid fibrils [29].

In this review, we will focus on protein aggregation in HD, which is a relatively rare disease (5–7 cases per 100 000 persons [30]), but its etiology is a mutation in a single gene. Therefore, studies on HD are more directly comparable than those on AD, PD, and ALS, all with predominantly sporadic and unclear etiologies. HD is caused by the expansion of a CAG repeat in the IT15 gene that codes for the Huntingtin (Htt) protein, resulting in the expansion of a poly-glutamine (polyQ) repeat in the N terminus of this protein. In HD pathology, N terminal fragments of polyQ-expanded Htt aggregate into oligomers and IBs [31]. The studies interpreting IBs as protective entities argue that oligomers, as the more toxic species, are sequestered into less toxic IBs [10,13,32,33]. By contrast, other studies propose that IBs are toxic to cells and important for the disease mechanism [34–36]. The toxicity of aggregates can be mediated either by loss- or gain-of-function effects [1]. It has been shown that expanded polyQ can misfold *in vitro* into different conformational states, which may have different neurotoxicity *in vivo* [37,38]. Such structural diversity is indeed recapitulated in the brains of HD mice, as amyloids in the striatum were associated with significantly higher toxicity and had a conformation different from other brain regions [37]. This supramolecular polymorphism may be a more general phenomenon for disease-related amyloids [39–42].

To clarify the role of aggregates in disease, many recent studies investigated the structure of aggregates *in vitro* at high resolution using fibrils either extracted from patients or generated *in vitro* [43]. The investigation of neurodegeneration in living cells is restricted to cell cultures and animal models, which can only partially recapitulate the disease phenotype [44,45]. To gain comprehensive understanding of these diseases, it is important to develop new tools and strategies to image patient-derived material. This will be discussed in the concluding remarks. In this review, we focus on methods with subcellular resolution to investigate the structure of IBs within their cellular environment: **conventional electron microscopy (EM)**, **super-resolution (SR) light microscopy (LM)**, and **cryo-electron tomography (cryo-ET)**.

## Conventional Electron Microscopy

Transmission electron microscopy (TEM) has enabled the investigation of cells and tissues at the nanoscale for about seven decades. Biological samples are intrinsically aqueous and thus not compatible with the vacuum of the electron microscope. In conventional EM this problem is overcome by chemical fixation, dehydration, and resin embedding of the cells or tissue. For contrast enhancement, samples are stained with heavy metals. The target thickness for TEM investigations is limited to a few hundred nm. Biological samples are regularly much thicker and are thus usually thinned down by microtome sectioning.

The first EM study of HD was published in 1997 and presented IBs in human brain (Figure 1A) [34]: IBs were described as highly heterogenous and were found mainly in the cytosol of neurons

## Glossary

**CLEM (Correlative Light and Electron Microscopy):** uses the strength of both methods – the ability to identify macromolecules by fluorescent light microscopy and the molecular resolution of electron microscopy to correlate micrographs of the same region of the sample.
**Conventional electron microscopy:** uses a transmission microscope that probes the sample with accelerated electrons, which have a resolution limit orders of magnitude better than visible light. The liquid content of biological matter is incompatible with the vacuum of an electron microscope, thus samples are chemically fixed, dehydrated, and plastic embedded and furthermore stained with heavy metals to increase contrast.
**Cryo-Electron Tomography (Cryo-ET):** a novel high-resolution method that is able to take 3D snapshots (tomograms) of the molecular landscape inside cells with an electron microscope. The essential point of this method – to keep the biological sample in its pristinely preserved, close-to-native state – is achieved by vitrification (cryo-preservation), which keeps all proteins and cellular structures in their original conformation at a certain point in time.
**Inclusion body (IB):** a large protein aggregate – pathognomonic for most neurodegenerative diseases. They contain the disease protein among others and are found in the cytosol and/or the nucleus. Their role in the disease pathology is a major topic of debate.
**Super-resolution light microscopy:** a group of light-microscopic techniques that circumvent Abbe's diffraction limit and thus reach higher resolution. There are two major branches of super-resolution microscopy: deterministic and stochastic approaches. These methods rely on the fluorescent labeling of the structure of interest.

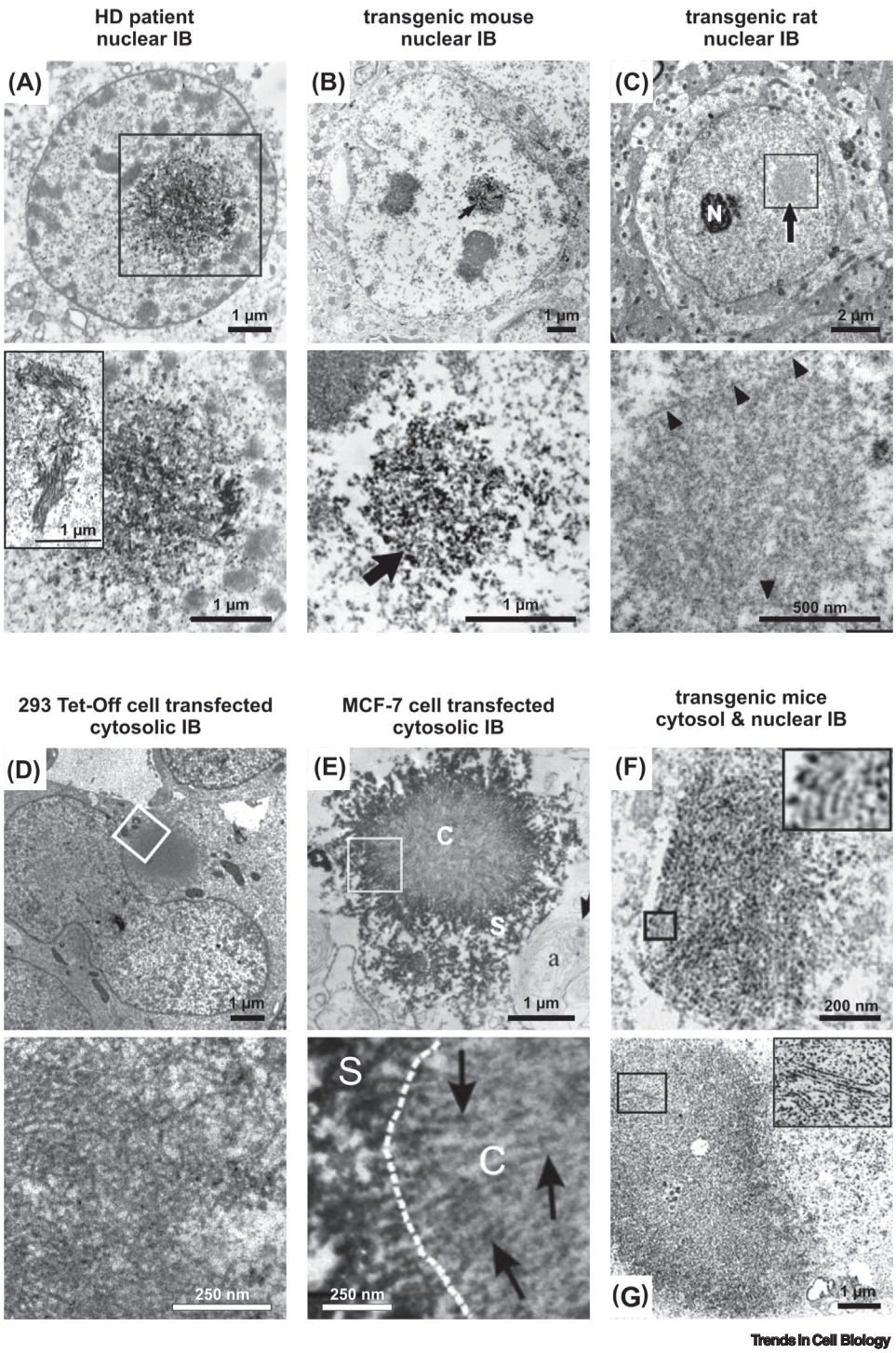


*(See figure legend at the bottom of the next page.)*

of adult patients, while nuclear localization was more frequent in patients with juvenile onset of HD. Cytosolic IBs were surrounded by organelles, mainly mitochondria, and not delimited by a membrane. To deepen the understanding of the ultrastructural architecture of Htt IBs, several studies further analyzed IBs in transgenic animal models [46–48] and transfected human cell lines [49,50] by conventional EM (Figure 1B–F). Both nuclear and cytosolic IBs were found in these model systems.

The visual appearance of the IBs was, however, heterogeneous between the different studies (see Table S1 in the supplemental information online): several studies described the IBs as substantially amorphous, containing granular and only a few fibrillar structures (Figure 1A–C) [34,46–48], while others observed fibrils more clearly (Figure 1D,E) [49,50]. It is difficult to explain this variance by the properties of the sample (Table S1), but it may be related to the sample preparation procedures. As for any microscopic method, the quality of the sample preparation determines the quality of the final image. Chemical fixation, dehydration, resin embedding, and staining with heavy metals are procedures that likely induce structural artifacts [51], particularly at the molecular level. The removal or substitution of water molecules inevitably denatures proteins through the loss of the hydration shell and causes soluble cytoplasmic components to precipitate onto membranes or fibrillar structures [52,53], leaving 'empty' white spaces in the micrographs. Thus, it is likely that differences in sample preparation procedures may have substantially contributed to the heterogeneity of IB ultrastructure in studies using conventional EM.

However, conventional EM allows analysis of patient-derived tissues and visualization of the localization and distribution of cellular IBs [34]. Furthermore, conventional EM allows immunogold labeling of structures to identify them in the plethora of structures in the cellular landscapes. Another advantage of this method is the potential to cover a larger volume by imaging multiple serial sections.

## Light Microscopy

Individual amyloid fibrils are too small to be visualized by conventional LM. SR techniques (Box 1) that work around Abbe's diffraction limit have been great advances in modern fluorescence

Figure 1. Comparison of Htt IBs in Model Systems and Patients Imaged by Conventional Electron Microscopy (EM). (A) Human neuronal intranuclear IB (hNII) in the cortex of a Huntigton's disease (HD) patient immunolabeled with anti-Htt antibody (Ab1). Upper: hNII in a cortical neuron appears as a dense aggregate with no limiting membrane separating it from the nucleoplasm. Lower: higher magnification of hNII shows the presence of labeled granules and filaments within the inclusion. Inset: serial section of hNII shows fibrils organized in random and parallel arrays. (B) Huntingtin within the neuronal nucleus of transgenic R6 mice. Discrete deposition of Htt115-156Q exon 1 within two neuronal intranuclear IBs (arrowheads) labeled by antibodies against huntingtin. (C) Intranuclear Htt51Q exon 1–15 IB of tgHD Sprague Dawley rat labeled with EM48 antibody. Upper: a striatal neuron showing a round intranuclear IB (large arrow) slightly larger than the neighboring nucleolus (N). Lower: at higher magnification, the membraneless IB reveals a granular and fibrillar (arrowheads) appearance. (D) Transfected 293 Tet-Off cells containing Htt83Q exon 1 IB, after expression for 3–5 days. Upper: cell containing a typical perinuclear inclusion body. Lower: at higher magnification (part of area boxed in upper figure), Htt83Q exon 1 fibrils with a diameter of roughly 10 nm can be observed. (E) Huntingtin IBs. MCF-7 cells were transiently transfected with an N terminal 969 amino acid long truncated, FLAG-tagged, 100Q Htt-construct (FH969–100Q) and immunostained for FLAG using the immunoperoxidase method. Upper: this cell contains one Flag-labeled Htt IB. Note the radiating fibrils in the core (C) and the less defined structure in the shell (S). Multilamellar-type autophagic bodies (a) abut the shell. Lower: higher magnification of the IB (boxed area in upper figure). The broken line is the approximate boundary between the shell (S), which is heavily labeled for Flag, and the core (C), which is not. There are radiating fibrils in the core (arrows). (F) Ultrastructural transmission electron microscopy analysis of CAG53b stained neuropil inclusion or dystrophic neurite (G) from the cortex of a Tet/HD94 mouse. Inset in (F) shows a 3.5× magnification of the indicated area. Inset in (G) shows a 2.5× magnification of the indicated area. (A) modified, with permission, from DiFiglia *et al*. [34]; (B) modified, with permission, from Davies *et al*. [46]; (C) modified, with permission, from Petrasch-Parwez *et al*. [48]; (D) modified, with permission, from Waelter *et al*. [50]; (E) modified, with permission, from Qin *et al*. [49]; (F,G) modified, with permission, from Díaz-Hernández *et al*. [59].

LM and offer the possibility to investigate dynamic cellular processes at resolutions below 100 nm [54–56].

### Super Resolution Methods

The mechanisms underlying Htt IB formation in the cell were studied by live-cell imaging using structured illumination microscopy (SIM) (Figure 2A) [57]. At first, small aggregates clustered in the cytosol chiefly by diffusion. Thus, in contrast to previous models, it was proposed that active transport via microtubules is not an important initiator of IB growth. Aggregates not only fuse, but can also undergo fragmentation (Figure 2B).

Cytosolic fibrillar aggregates of ~100 nm in diameter and ~1–2 μm in length were observed in fixed neuronal-like differentiated PC12 cells (derived from a pheochromocytoma of the rat adrenal medulla) using single-molecule active-control microscopy, besides the IBs and the diffuse pool of monomers and oligomers (Figure 2C) [58]. Individual huntingtin fibrils have a diameter of 8 nm [34,46,48–50,59–61] and therefore the aggregates observed in this study likely correspond to fibril bundles and not to single fibrils. Later on, the authors used stimulated emission depletion live-cell imaging to show that such large fibrillar Htt exon 1 aggregates appear all over the cytosol after the initial aggregation of mutant Htt into IBs (Figure 2D) [62]. The fact that these fibrils appeared only in advanced growth stages of the IB was interpreted as a probable failure of the cellular degradation system in preventing the nucleation of the toxic aggregated protein species.

Another study examined the aggregation dynamics of IBs in living mouse ES-D3 cells (mouse embryonic multipotent stem cells) and mouse STH*dh* striatal cells (mouse striatal cell line) by

#### Box 1. Super-Resolution (SR) Light Microscopy (LM) Methods

SR-LM is a set of novel imaging techniques that circumvent the diffraction limit of light and reach a resolution down to well below 100 nm. Two major groups of SR microscopy can be distinguished: stochastic and deterministic approaches. To visualize the structure of interest, proteins need to be fluorescently labeled. Live-cell imaging is a big advantage of LM methods; to increase precision, samples can also be fixed.

Structured illumination microscopy (SIM) [107] is a deterministic SR technique. Two laser beams interfere to create a stripe pattern close to the resolution limit with which the sample is illuminated. The interference of the pattern frequency with high frequency features of the sample are computationally decoded from the resulting images to reconstruct high resolution images. SIM can be used for live-cell imaging with high temporal (10–30 Hz) and spatial resolution (80–100 nm) with conventional fluorophores and low phototoxicity. The imaging depth is sufficient for multilayered tissues.

Single-molecule active control microscopy (SMACM) [108], also often called single-molecule localization microscopy, is a group of stochastic SR techniques, including photoactivated localization microscopy (PALM), fluorescence photoactivation localization microscopy (F-PALM), super-resolution optical fluctuation imaging (SOFI), and stochastic optical reconstruction microscopy (d)STORM, that have the advantage of reaching a particularly high resolution, down to 10–20 nm. This is achieved by fitting the point spread function to the image of isolated fluorophores. The localization precision is only limited by the intensity of the emitter. Typically, the fluorophores of biological samples are too close to each other to be detected individually. By activating stochastically only a sparse subset of emitters at a time, their precise localization can be achieved. These methods are typically rather slow (minutes scale), compared with biological time scales and thus less optimal for live-cell imaging. However fast-switching dyes [109] and scientific complementary metal-oxide-semiconductor (sCMOS) cameras [110] allow live-cell imaging with subsecond frame rates. The imaging depth is sufficient for single cells.

Stimulated emission depletion microscopy (STED) [111,112] is also a deterministic SR technique that utilizes two laser pulses: an excitation beam superimposed with a depletion beam with an intensity minimum in the focal center that shapes the effective scanning spot size by depletion of peripheral emitter fluorescence. STED reaches a spatial resolution around 40–50 nm, with frame rates in the tens of seconds scale. Phototoxicity needs to be considered due to high laser intensities. The imaging depth is sufficient for multilayered tissues.

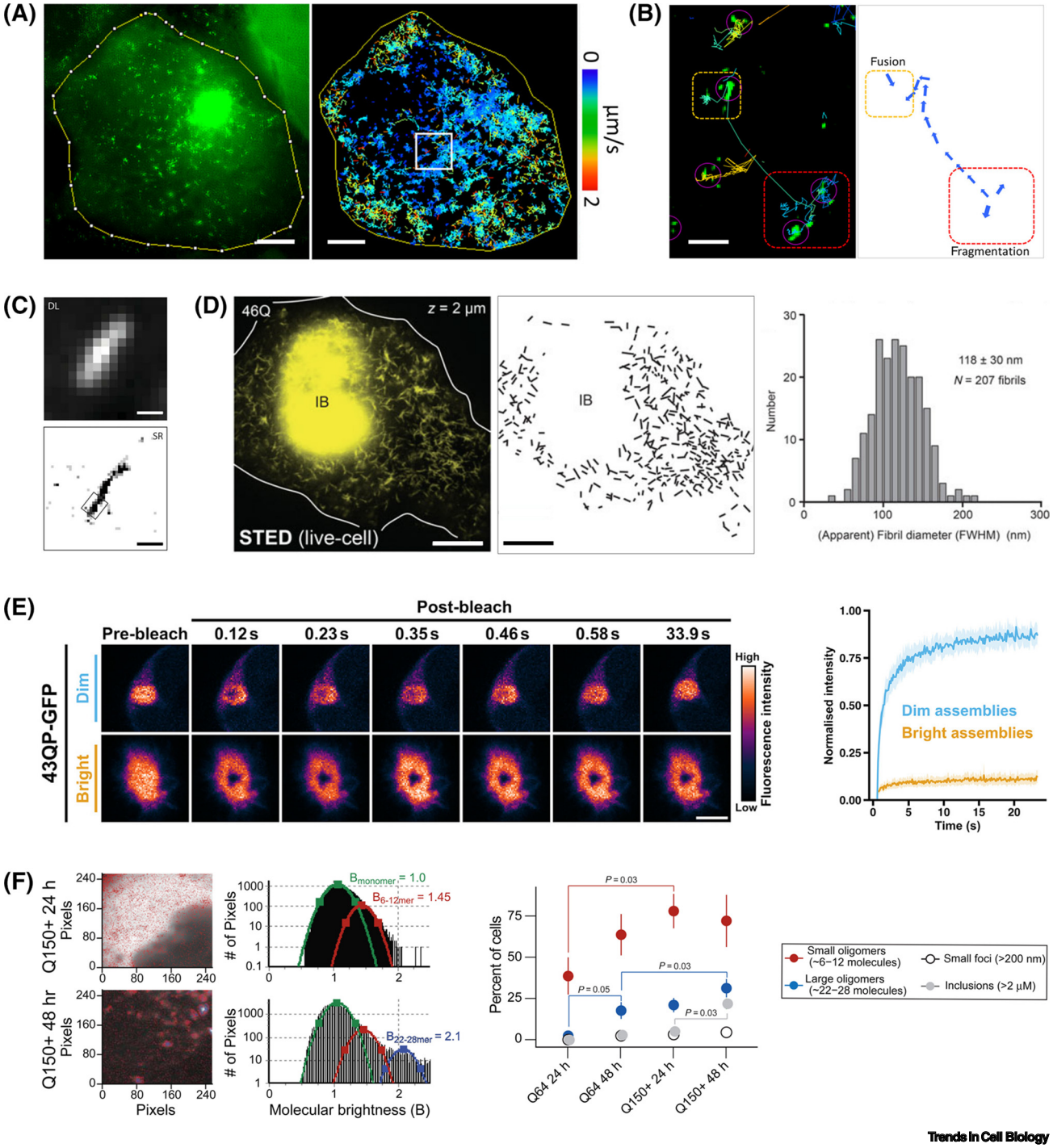


Figure 2. Investigation of Huntingtin Inclusion Bodies (IBs) by Novel Light Microscopy (LM) Techniques. (A) High-speed structured illumination microscopy (SIM) recordings of intracellular aggregate dynamics. All small aggregates are subjected to dramatic random movements, which lead to collisions and contacts among clusters. Using a single particle tracking algorithm, individual particles were identified and their trajectories were analyzed in time at a frame rate of 5 Hz (right). The velocity spectrum (left). Scale bar, 5 μm. (B) Poly-glutamine (PolyQ) aggregates undergo frequent fusion and fragmentation events in the cell. Aggregate motion includes both active and passive transport components. The purple circles highlight regions where small clusters were identified in the automated analysis. The broken

*(Figure legend continued at the bottom of the next page.)*

single-molecule active-control microscopy. With this method, three distinct dynamic states were differentiated: (i) fast diffusion, (ii) dynamic clustering, and (iii) stable aggregation [63]. The results provide insights into mutant Htt aggregate formation and how these structures may disrupt gene-control mechanisms in neuronal cells. Large, stable aggregates in the nucleus form 'sticky' decoy traps that impair the function of key regulators of gene expression involved in neurological disorders.

### Other Light Microscopic Approaches

To monitor the aggregation properties of Htt exon 1 with different polyQ lengths in cells, Kim *et al*. [12] applied a single molecule fluorescence fluctuation spectroscopy technique known as numbers and brightness (N&B) [64] on Neuro2a cells expressing Htt exon 1 (Neuro2a cells derive from a mouse neuroblastoma). The N&B method uses intensity fluctuations to estimate the average number of fluorescent molecules per pixel and their oligomerization state (brightness). With this method different aggregation states can be distinguished. Thereby the aggregation process was followed over time from monomers and small oligomers (6–12 molecules), to large oligomers (22–28 molecules), and eventually to macroscopic IBs (>2 μm). Interestingly, this analysis showed that the formation of IBs did not substantially reduce the concentration of oligomers.

Using fluorescence recovery after photobleaching (FRAP), Peskett *et al*. [60] investigated the nature of the signal intensity of bright and dim IBs formed by Htt exon 1 in *Saccharomyces cerevisiae* and human embryonic kidney (HEK293) cells. FRAP uses a laser to bleach fluorescent molecules in a defined volume; depending on the diffusivity/mobility of the fluorescent molecules in this volume, the signal intensity may recover. The dim assemblies showed high internal mobility and were thus considered liquid-like macroscopic structures, which gradually convert over time into the brighter IBs that behaved like solids (Figure 2E). With conventional EM, the authors confirmed that solid-like IBs were fibrillar, in contrast to the amorphous liquid-like IBs.

These studies show that SR-LM, but also advanced diffraction-limited fluorescent imaging, are invaluable tools for the investigation of dynamic processes in living cells, in particular for the study of the structural progression of protein aggregates *in situ.* However, as the resolution of these methods is limited, they cannot fully clarify IB ultrastructure.

## Cryo Electron Tomography

In contrast to conventional EM, cryo-ET is capable of imaging cellular structures at molecular resolution while preserving the sample in an unperturbed, close-to-native state.

To prevent the water from evaporating in the microscope vacuum, physical fixation through very rapid freezing ($10^4$–$10^5$ K/s) results in the formation of amorphous ice [65–67]. This process is called vitrification and transforms liquid water into a glass-like solid, not allowing water molecules to

orange and red rectangles indicate regions where fusion and fragmentation take place, respectively. Scale bar, 2 μm. (C) Small aggregate, imaged with super-resolution (SR) microscopy, based on the light-induced blinking of single eYFP fused to Htt exon1. Upper: diffraction-limited (DL) image. Lower: SR reconstruction of the structure as histograms of localizations. (D) Fibrillar structures Imaged by live-cell stimulated emission depletion microscopy (STED). Left: example of fibrillar structures coexisting with inclusion bodies, imaged by live-cell SR STED microscopy. Middle: outlines of identifiable linear fibril segments. Right: width distribution of $N = 207$ individual cross-sections of fibrils [full width at half maximum (FWHM) of Gaussian fit]. (E) Fluorescence recovery after photobleaching (FRAP) analysis of Htt exon1 inclusion bodies. Left: FRAP experiment showing high Htt exon1 mobility in dim assemblies but not in bright assemblies. Scale bar, 3 μm. Right: averaged FRAP recovery curves. Shaded areas represent 95% confidence intervals. (F) Numbers and brightness (N&B) analysis of cells expressing Q18, Q64, and Q150+ for 24 and/or 48 h. Left: the left images show the pixel selection map of the analyzed cell, alongside the histograms of the number of pixels per molecular brightness. The green/red/blue curves indicate monomers/6-12mers/22-28mers. Middle and right: characterization of cell populations in progressive stages of aggregation. The fraction of cells containing small oligomers (red circles) and large oligomers (blue circles) were quantified using N&B; cells containing aggregates (gray circles) and inclusions (black circles) were quantified using conventional LM. (A,B) modified, with permission, from Lu *et al*. [57]; (C) modified, with permission, from Sahl *et al*. [58]; (D) modified, with permission, from Sahl *et al*. [62]; (E) modified, with permission, from Peskett *et al*. [60]; (F) modified, with permission, from Kim *et al*. [12].

reorganize into crystals. The latter would damage and/or distort biological structures due to volume expansion and the exclusion of solvents. Vitrification preserves cellular samples in a close-to-native state, fully hydrated, unstained, with halted Brownian motion. Molecular structures are well preserved in their physiological state, shape, and conformation, allowing high resolution imaging.

Electron micrographs are 2D projections of the entire 3D object. Thus, features from different layers are superimposed, making it difficult to interpret these images in their third dimension. Cryo-ET provides 3D volumes of the sample, by computationally reconstructing many projection images recorded by tilting the sample in the beam.

In the recent past, three major technological advances refined the cryo-ET methodology (Box 2) and thereby made new ways of studying cellular processes possible: firstly, direct electron detectors [68–70] increase the signal-to-noise ratio (SNR) and allow for correcting beam-induced motion, which otherwise limits resolution. Secondly, the development of the cryo-focused ion beam (cryo-FIB) technology, which opens windows into the interior of frozen-hydrated vitrified cells by producing thin lamellas [71,72]. And finally, the development of the Volta-phase plate, which enables imaging of the sample close to focus and with maximum contrast [73,74].

These technological advances make cryo-ET uniquely capable of investigating IBs *in situ*, in their pristinely preserved cellular environment, at molecular resolution [75]. The first study dissecting

### Box 2. Workflow of Correlative Cryo-Electron Tomography (Cryo-ET)

The aim of cryo-ET is to visualize the unperturbed cellular landscape in its full complexity at molecular resolution [113]. Cellular processes, macromolecules, and their interactions, as well as pathological conditions, can be observed in their native environment. The preservation of biological matter in a close-to-native state is achieved by vitrification: a very rapid freezing of the sample (see main text), providing optimal structural conservation.

**Targeting the Structure of Interest (Correlative Microscopy)**

The large landscape of many hundreds to thousands of eukaryotic cells grown or deposited on an EM grid (Figure IA) typically requires identification of cells containing the structure of interest (e.g., protein aggregates). Furthermore, localization of subcellular features is challenging because the volume of a eukaryotic cell (several thousand $\mu m^3$) is much larger than the volume of a tomogram (around 1 $\mu m^3$) (Figure IB) of the structure of interest.

Targeting the structure of interest can be achieved by fluorescently labeling the cellular feature and **correlative light and electron microscopy (CLEM)** [114]: the vitrified cells are imaged by fluorescence cryo-LM and consecutively by cryo-scanning electron microscopy (SEM). By superimposing (indicated by Σ) the images obtained by both microscopes (Figure IA,B) the subcellular location of a structure of interest can be determined with a precision of about 200–300 nm [115]. Recent approaches using SR-LM yield higher localization precision and combine the power of both methods: the high resolution of cryo-ET and the ability to identify the visualized molecular species [116].

**Opening Windows into the Cell (Lamella Preparation)**

The main limitation of TEM is the sample thickness. Electrons interact strongly with matter, so that only biological samples with a thickness of ≤500 nm can be imaged with sufficient signal-to-noise ratio (SNR), although thinner samples (around 200 nm) are preferable. As eukaryotic cells are typically much thicker, the region of interest needs to be thinned down (Figure IC). In a cryo-FIB/SEM dual-beam instrument, a thin lamella, containing the structure of interest (Figure ID), is prepared with a focused ion-beam from a single cell [71].

**Tomography**

The lamella containing the structure of interest is transferred into a cryo-TEM. A series of projections is acquired by tilting the sample. These projections are computationally reconstructed into a 3D-representation of the sample: the tomogram. The imaging electron-dose is limited in cryo-EM due to sample damage, thereby limiting the contrast and SNR. Two recent developments, direct imaging detectors and the Volta-phase-plate, drastically increase both parameters. Recurrent structures in the tomogram can be averaged by sub-tomogram averaging [117,118] to improve SNR and resolution.

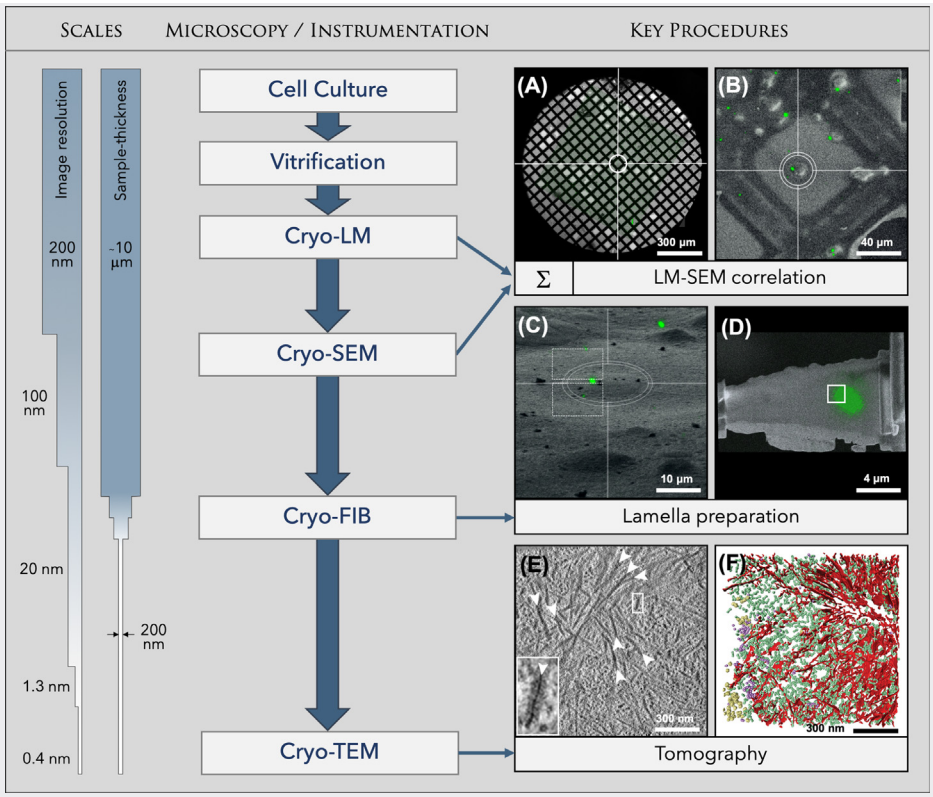


Figure I. Workflow of Correlative Cryo-Electron Tomography (Images A–F: modified, with permission, from [91]).

pathological protein aggregation *in situ* used the aforementioned advanced cryo-ET methods to investigate polyQ-expanded Htt exon1 IBs in their cellular environment of primary mouse neurons and immortalized human cells [61].

## IB Architecture and Ultrastructure

Primary mouse neurons and HeLa cells expressed GFP-tagged Htt Exon 1 (Htt97Q-GFP) and were processed following the workflow presented in Box 2 to generate tomograms of the IBs. Htt97Q-GFP inclusions, roughly spherical and ~3 µm in diameter, were mostly cytosolic but also occasionally found in the nucleus. Both cytosolic and nuclear inclusions were formed by mostly radially arranged amyloid-like fibrils with a diameter of 7–8 nm and a length of 100–200 nm, yet neither granular nor amorphous material was observed (Figure 3A,B). Despite the dense appearance of the IB network, the fibrils occupied less than 3% of the IB volume, resembling a gel-like structure. On the contrary, the expression of a similar Htt Exon 1 construct in *S. cerevisiae* led to the formation of amorphous IBs [76]. Thus, the morphology of Htt Exon1 aggregates varies in different cellular environments, possibly due to differences in the protein quality control machineries [77,78]. These data show that cryo-ET can efficiently distinguish different IB architectures.

Images of vitrified biological matter reflect snapshots of the physiological condition. Thus, the analysis of the curvature of fibrils provides insight into their mechanical properties (flexibility)

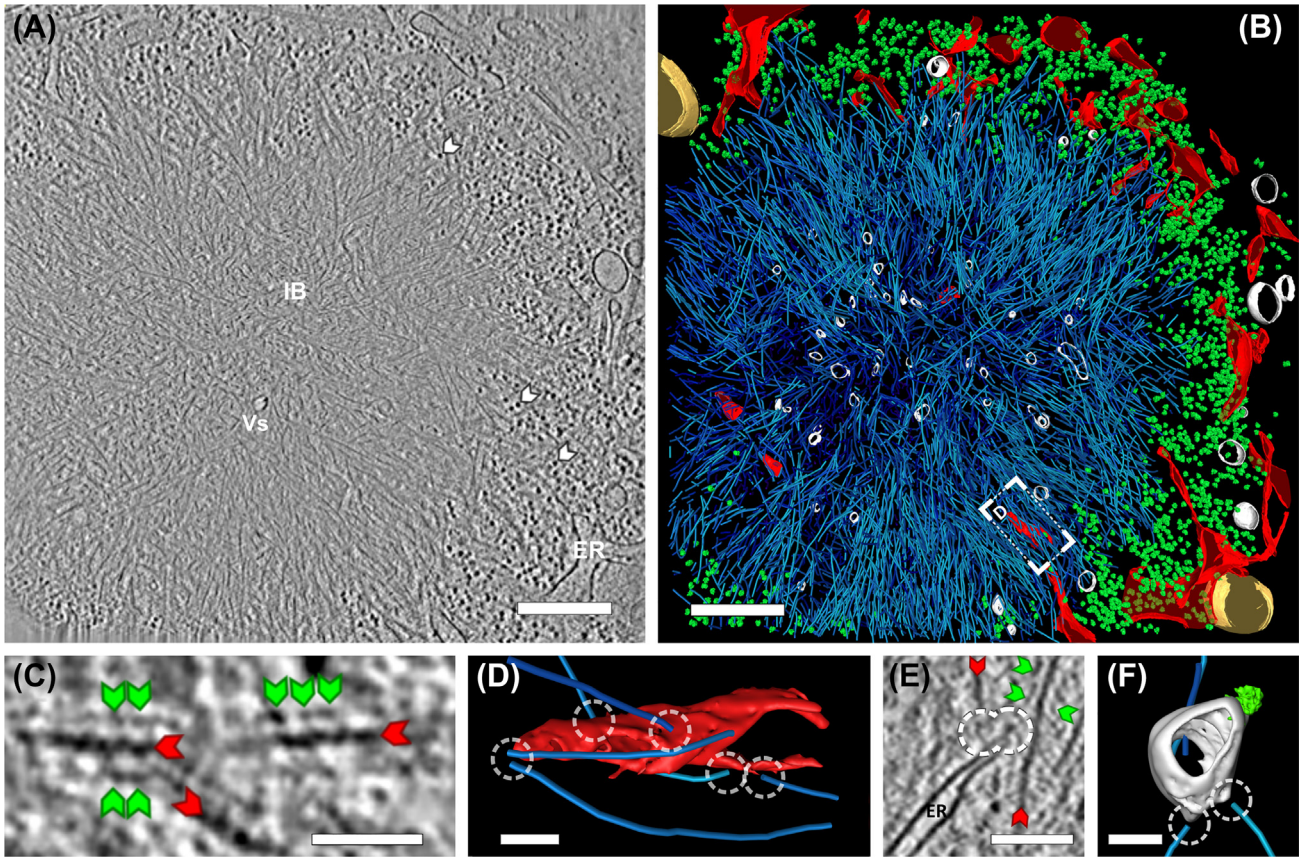


Figure 3. Cytosolic Inclusion Bodies (IBs) of Mutant Huntingtin Visualized by Cryo-Electron Tomography (Cryo-ET). (A) Tomographic slice of an IB (Htt97Q-GFP inclusion body) in an Htt97Q-GFP-transfected mouse primary neuron. The cytoplasmic electron dense particles are ribosomes (white arrowheads). (B) 3D rendering of the tomogram shown in (A). Endoplasmic reticulum (ER) membranes (red), Htt97Q-GFP fibrils (cyan), ribosomes (green), vesicles (Vs) (white), and mitochondria (gold). Note that the core of the IB is largely devoid of ribosomes, which are abundant at the IB periphery. Scale bars, 400 nm in (A) and (B). (C) High-magnification image of Htt97Q-GFP fibrils (red arrowheads) decorated by globular densities (green arrowheads). Scale bar, 30 nm. (D) Magnified rendering of the region marked in (B) showing interaction sites (white circles) between Htt97Q-GFP fibrils and the ER membrane. Scale bar, 50 nm. (E) Tomographic slice showing Htt97Q-GFP fibrils (red arrowheads) decorated by globular densities (green arrowheads) interacting with cellular membranes in Htt97Q-GFP-transfected neurons. Scale bar, 100 nm. (F) 3D rendering of a vesicle trapped in an IB. Note the membrane-bound ribosome and the high curvature of the vesicle membrane at the sites of interaction with fibrils. Scale bar, 100 nm. (A–F) modified, with permission from Bäuerlein *et al.* [61].

at physiological temperature: the Htt fibrils persistence length (stiffness) was approximately 2.6 μm, in the range of actin and also Tau filaments [72,79].

The resolution in this study was high enough to identify globular densities decorating the fibrils. These densities had a diameter of ~6 nm, consistent in size with GFP-dimers (Figure 3C). Control analyses of Htt97Q IBs without a GFP tag revealed similar fibril diameter and length but without the globular densities. In general, fibrils were always observed as part of inclusions, suggesting that IBs are the main site of fibril growth in the cell [80]. However, since a tomogram covers only a small percentage of the entire cell, isolated fibrils in other parts of the cell could have been missed, as well as small fibrils (<50 nm) that cannot be reliably detected. The gel-like IB core was largely devoid of large macromolecules such as ribosomes, which were abundant at the IB periphery.

### Cellular Interactions of IBs

Strikingly, fibrils contacted membranes of organelles at the IB periphery (Figure 3D,E), including mitochondria, lysosomes, and, most prominently, the endoplasmic reticulum (ER). At the sites of contact, the impingement of fibrils caused high membrane curvature. Ribosome-free ER-tubes often protruded into the IB, interacting extensively with the fibril network (Figure 3B,D). Numerous irregular shaped vesicles were embedded in most cytosolic inclusions at sites of interaction with organelles. Many of these vesicles were contacted by fibrils at regions of extreme membrane curvature, suggesting that they resulted from fibril-mediated disruption of organelles. Some of these trapped vesicles carried ribosomes (Figure 3F), suggesting that they originated from ruptured ER membranes. Interestingly, the ability of amyloid fibrils to disrupt membranes has also been previously observed by cryo-ET *in vitro* [81]. These observations with molecular resolution guided the way to further analyses with fluorescence LM that supported these findings and showed that the fibril–membrane interactions at IBs significantly disrupt the organization and dynamics of the ER. Nuclear inclusions were indistinguishable from cytosolic ones in terms of overall architecture, but did not contain any vesicles, nor did the fibrils contact the inner nuclear membrane. By taking advantage of the latest advancements of cryo-ET, this study showed that fibril–membrane interactions significantly disrupt both the organization and the dynamics of the ER, thus pointing to a pathogenic role of IBs in HD [82].

### Limitations of Cryo-ET

The optimal sample for the investigation of neurotoxic protein aggregates would be viable human brain tissue from patients. Besides the challenges to retrieve living human brain tissue for this purpose (which will be discussed in the next section), there are two main limitations that restrict the sample size for cryo-ET analyses: vitrification and sample thinning.

#### *Vitrification*

Plunge freezing [83] is the most widely used vitrification method in cryo-ET to vitrify single cells. For larger samples like tissue, high-pressure freezing [66] is often used, allowing vitrification for thicknesses up to a few 100 µm. Larger samples will form ice crystals in their core due to insufficient cooling rates. This means that with current methods, only small tissue pieces (i.e., biopsies) could potentially be vitrified, but not larger samples in their entirety.

#### *Sample Thinning*

One way of thinning samples is mechanical cryo-sectioning, which can produce thin sections from cells and tissue. However, this method is associated with adverse artifacts, including strong and irregular deformations of cellular structures [84–86]. Currently, cryo-FIB [71,87] has become the gold standard to thin down vitrified cellular specimens. Although this works well for single cultured cells, for much larger material like tissue, FIB-thinning is very time consuming and technically challenging. Recently, the cryo-FIB technology has been extended to prepare lamellas from tissue specimens: the lamella can be lifted out of the material, without the need to mill away large sample volumes [88–90].

## Concluding Remarks and Future Perspectives

In summary, two methodological aspects are essential for the reliable investigation of the ultrastructure and the dynamics of neurotoxic protein aggregates: (i) imaging methods with high spatial and temporal resolution; and (ii) sample preparation procedures that minimize disturbances of the pathophysiological cellular situation and deliver reliable, reproducible, and unambiguous results.

Each method has its advantages and limitations. SR-LM has played an important role in the past 10 years in the investigation of the structural progression of protein aggregates *in situ* [54]. It is a

particularly valuable method to analyze dynamic processes in living cells. However, SR methods have two main limitations: they only allow visualization of fluorescently labeled structures but not their local environment (but see [124]) and, secondly, the resolution is limited to 10–100 nm.

EM can achieve a resolution two orders of magnitude higher. Consequently, it can investigate the ultrastructure of protein aggregates *in situ*. However, the sample preparation of conventional EM suffers from harsh procedures that are very likely to induce structural alterations, particularly at the molecular level. Thus, conventional EM is, in general, incompatible with high-resolution imaging of biological specimens, which is reflected by the inconsistent observations of Htt IBs using this method (Figure 1 and Table S1). By contrast, the sample preparation for cryo-ET is capable of preserving the sample in a close-to-native state, making cryo-ET ideally suited for the ultrastructural investigation of biological specimens.

The recent advancements of cryo-ET enabled the direct visualization of the native ultrastructure of IBs and their cellular interactions [61,91,125,126]. The major advantage of this method is the three-dimensional representation of the cellular landscape at molecular resolution, depicting all cellular structures, not only labeled components.

The controversial debate about the relevance of oligomers and IBs in neurodegenerative diseases has not been resolved. However, the high-resolution imaging methods described in this review have provided new insights to this debate beyond the known toxicity of oligomers. SR techniques analyzed the dynamics of IBs and the aggregation process [12,57,58,60,62]. The evidence derived from cryo-ET studies visualized for the first time the destructive potential of IBs [61,91].

Looking into the future, there are emerging technologies that may receive further attention in the field (Box 3).

## Outstanding Questions

Can we use SR-LM and cryo-ET synergistically to study the dynamics and molecular architecture of protein aggregates?

Can we adapt cryo-ET methodology to enable examining patient-derived samples under close-to-native conditions?

Can an integrative multiscale imaging approach contribute to the development of new therapies for neurodegenerative diseases?

### Box 3. Emerging Methods

Cryo ptychographic X-ray computed tomography (cryo-PXCT) [119,120] is a method that uses synchrotron radiation to visualize 3D subcellular features at a resolution of ~100 nm of specimens with a thickness approaching 100 µm. The resolution is low in comparison with the techniques described earlier, yet the method has the advantage of allowing a frozen-hydrated tissue sample (e.g., brain tissue from animal models or patients) to be imaged in its entirety without labeling. Furthermore, after cryo-PXCT imaging, samples may potentially be further imaged by the high resolution methods described in this review. This method could contribute insights into tissue-specific alterations (e.g., neuronal connectivity, synaptic changes, and myelination).

In-cell nuclear magnetic resonance (in-cell NMR) can provide atomic resolution of intracellular protein structures and delivered valuable information about the cellular aggregation of α-synuclein [121]. The data of in-cell NMR reflects not a single-cell analysis, but rather an ensemble-average of the population, where the signal originates from many molecules in many cells.

Stimulated Raman scattering of selective deuterium labeling allows live-cell imaging and quantification of polyQ aggregates [122]. Deuterated glutamine renders fluorescent labeling unnecessary. Miao *et al*. could measure absolute concentrations of sequestered mutant Htt and other proteins within the same aggregate and discovered that the percentage of mutant Htt increases as the inclusion grows [122]. Since glutamine can cross the blood–brain barrier, an application of this method on animal models and hypothetically on patients may be possible.

Correlative 3D super-resolution (SR) and scanning electron microscopy (SEM)-based imaging [123] is a method that combines the strength of SR-LM in identifying proteins and the ability of SEM to visualize large cellular volumes. Cells are vitrified and imaged in 3D by SR methods (3D-SIM and SMACM) under cryo-conditions. Thereafter the frozen cells are dehydrated and embedded in resin by freeze substitution and finally stained by heavy metals to increase contrast. In a dual-beam FIB-SEM instrument, the focused ion-beam removes consecutively thin layers and so a large volume of the cell is imaged by the electron beam with an isotropic resolution of 4–8 nm. If this method is further developed to keep cells vitrified for the SEM-based imaging, nonlinear deformation artifacts caused by freeze substitution could be avoided, however, probably with a forfeit in contrast.

Besides the methodological approaches, it is also crucial to consider the biological system that is used to investigate the disease mechanisms. Valuable insights into neurodegenerative diseases have been obtained from cell cultures and animal models. Nevertheless, after more than 110 years of research, there is not sufficient understanding of the pathomechanisms involved. As a result, not a single pharmaceutical substance to date could modify the progression nor the mortality of these diseases and pharmacological strategies are restricted to symptomatic treatments. This implies that there is a large gap in knowledge of basic disease mechanisms. To reach a comprehensive, pathophysiological understanding of neurodegenerative diseases, it seems crucial to investigate the genuine disease situation. All cellular and animal models recapitulate only partially the disease phenotypes [44,45]: for example, a single genetic mutation is typically used to model the disease, while most patients do not have such mutations. The pathogenic protein is overexpressed in model systems to observe aggregation in a reasonable timeframe, contrary to patients that express this protein at normal level over decades. Model systems do not exhibit the temporal speed of the disorder, nor the spectrum of pathologies and symptoms, which challenges the translation of new findings from disease models to the clinic.

Thus, the future success of understanding these pathologies may depend on the investigation of vital patient-derived material. However, postmortem tissue is not suitable for high-resolution studies, as brain tissue is extremely sensitive to anoxia and rapidly develops into brain death due to global ischemia in the dying patient. Irreversible cerebral damage develops rapidly, leading to a drastic decrease of survival in minutes if an individual is not resuscitated [92]. Furthermore, the chance of a favorable neurological outcome of a surviving patient after 30 min of resuscitation is vanishingly low [93], indicating major neuronal damage. Substantial structural alterations, affecting most organelles and cytosolic structures, have been observed in the first minutes to hours after global ischemia [94–97]. And importantly, cerebral ischemic injury and neurodegenerative disorders share many commonalities [94]. Thus, studies using high-resolution methods on postmortem tissue [98,99] image a cellular situation in which the neurodegenerative pathologies cannot be distinguished from postmortem artifacts and should thus be taken with caution.

This emphasizes the necessity of the vitality of patient-derived material: to be able to analyze unaltered samples, they need to be collected from living patients. Brain biopsies are, due to ethical considerations, restricted to therapeutic interventions (diagnostic biopsies, resection of therapy refractory epilepsy). However, other tissues are more easily available and single cells of these can be reprogrammed via induced pluripotent stem cells (iPSC) into neuronal cells [100]. However, iPSC-derived neurons failed to develop IBs in late-onset disorders [101], which may be due to an epigenetic reset of the donor age [102]. Thus, further developments and new strategies are necessary, as, for example, the direct conversion [103] that circumvents the epigenetic resetting or the induced aging of iPSC-derived neurons [104–106].

In this review, we have presented and discussed novel high resolution methods with close-to-native preparation methods that can be applied to patient-derived material. Combining these approaches holds high potential for major breakthroughs in understanding neurodegenerative diseases and perhaps may contribute to the development of effective treatments (see Outstanding Questions).

## Acknowledgments

**Dedicated to the memory of Professor Dr. rer. nat. Edmund Bäuerlein (1932–2019).**

F.J.B.B., R.F-B., and W.B. have received funding from the European Commission (FP7 GA ERC-2012-SyG_318987-ToPAG). R.F-B. acknowledges funding from the Deutsche Forschungsgemeinschaft (DFG, German Research Foundation)

through Germany's Excellence Strategy, EXC 2067/1- 390729940. We thank Dorothy Zhao for critically reading the manuscript.

## Supplemental Information

Supplemental information associated with this article can be found online at https://doi.org/10.1016/j.tcb.2020.08.007

## References

1. Hipp, M.S. *et al.* (2014) Proteostasis impairment in protein-misfolding and -aggregation diseases. *Trends Cell Biol.* 24, 506–514
2. Ross, C.A. and Poirier, M.A. (2004) Protein aggregation and neurodegenerative disease. *Nat. Med.* 10, S10–S17
3. Ross, C.A. and Margolis, R.L. (2005) Neurogenetics: insights into degenerative diseases and approaches to schizophrenia. *Clin. Neurosci. Res.* 5, 3–14
4. Iadanza, M.G. *et al.* (2018) A new era for understanding amyloid structures and disease. *Nat. Rev. Mol. Cell Biol.* 19, 755–773
5. Mroczko, B. *et al.* (2018) Amyloid β oligomers (AβOs) in Alzheimer's disease. *J. Neural Transm. (Vienna)* 125, 177–191
6. Naseri, N.N. *et al.* (2019) The complexity of tau in Alzheimer's disease. *Neurosci. Lett.* 705, 183–194
7. Shafiei, S.S. *et al.* (2017) Tau oligomers: cytotoxicity, propagation, and mitochondrial damage. *Front. Aging Neurosci.* 9, 83
8. Bengoa-Vergniory, N. *et al.* (2017) Alpha-synuclein oligomers: a new hope. *Acta Neuropathol.* 134, 819–838
9. Hergesheimer, R.C. *et al.* (2019) The debated toxic role of aggregated TDP-43 in amyotrophic lateral sclerosis: a resolution in sight? *Brain* 142, 1176–1194
10. Arrasate, M. and Finkbeiner, S. (2012) Protein aggregates in Huntington's disease. *Exp. Neurol.* 238, 1–11
11. Finkbeiner, S. (2011) Huntington's disease. *Cold Spring Harb. Perspect. Biol.* 3, a007476
12. Kim, Y.E. *et al.* (2016) Soluble oligomers of polyQ-expanded huntingtin target a multiplicity of key cellular factors. *Mol. Cell* 63, 951–964
13. Leitman, J. *et al.* (2013) Soluble forms of polyQ-expanded huntingtin rather than large aggregates cause endoplasmic reticulum stress. *Nat. Commun.* 4, 2753
14. MacDonald, M.E. *et al.* (1993) A novel gene containing a trinucleotide repeat that is expanded and unstable on Huntington's disease chromosomes. *Cell* 72, 971–983
15. Sánchez, I. *et al.* (2003) Pivotal role of oligomerization in expanded polyglutamine neurodegenerative disorders. *Nature* 421, 373
16. Schaffar, G. *et al.* (2004) Cellular toxicity of polyglutamine expansion proteins: mechanism of transcription factor deactivation. *Mol. Cell* 15, 95–105
17. Scherzinger, E. *et al.* (1997) Huntingtin-encoded polyglutamine expansions form amyloid-like protein aggregates *in vitro* and *in vivo*. *Cell* 90, 549–558
18. Ross, C.A. and Poirier, M.A. (2005) What is the role of protein aggregation in neurodegeneration? *Nat. Rev. Mol. Cell Biol.* 6, 891–898
19. Delenclos, M. *et al.* (2019) Cellular models of alpha-synuclein toxicity and aggregation. *J. Neurochem.* 150, 566–576
20. Goedert, M. *et al.* (2017) Propagation of Tau aggregates and neurodegeneration. *Annu. Rev. Neurosci.* 40, 189–210
21. Jouanne, M. *et al.* (2017) Tau protein aggregation in Alzheimer's disease: an attractive target for the development of novel therapeutic agents. *Eur. J. Med. Chem.* 139, 153–167
22. Oberstadt, M. *et al.* (2018) TDP-43 and cytoskeletal proteins in ALS. *Mol. Neurobiol.* 55, 3143–3151
23. Prasad, A. *et al.* (2019) Molecular mechanisms of TDP-43 misfolding and pathology in amyotrophic lateral sclerosis. *Front. Mol. Neurosci.* 12, 25
24. Reiss, A.B. *et al.* (2018) Amyloid toxicity in Alzheimer's disease. *Rev. Neurosci.* 29, 613–627
25. Wong, Y.C. and Krainc, D. (2017) Alpha-synuclein toxicity in neurodegeneration: mechanism and therapeutic strategies. *Nat. Med.* 23, 1–13
26. Goedert, M. (2004) Tau protein and neurodegeneration. *Semin. Cell Dev. Biol.* 15, 45–49
27. Gao, J. *et al.* (2018) Pathomechanisms of TDP-43 in neurodegeneration. *J. Neurochem.* Published online ebruary 27, 2018. https://doi.org/10.1111/jnc.14327
28. Querfurth, H.W. and LaFerla, F.M. (2010) Alzheimer's disease. *N. Engl. J. Med.* 362, 329–344
29. Rochet, J-C. and Lansbury, P.T. (2000) Amyloid fibrillogenesis: themes and variations. *Curr. Opin. Struct. Biol.* 10, 60–68
30. Walker, F.O. (2007) Huntington's disease. *Lancet* 369, 218–228
31. DiFiglia, M. *et al.* (1995) Huntingtin is a cytoplasmic protein associated with vesicles in human and rat brain neurons. *Neuron* 14, 1075–1081
32. Bucciantini, M. *et al.* (2002) Inherent toxicity of aggregates implies a common mechanism for protein misfolding diseases. *Nature* 416, 507
33. Haass, C. and Selkoe, D.J. (2007) Soluble protein oligomers in neurodegeneration: lessons from the Alzheimer's amyloid β-peptide. *Nat. Rev. Mol. Cell Biol.* 8, 101
34. DiFiglia, M. *et al.* (1997) Aggregation of huntingtin in neuronal intranuclear inclusions and dystrophic neurites in brain. *Science* 277, 1990–1993
35. Pieri, L. *et al.* (2012) Fibrillar α-synuclein and huntingtin exon 1 assemblies are toxic to the cells. *Biophys. J.* 102, 2894–2905
36. Stefani, M. and Dobson, C.M. (2003) Protein aggregation and aggregate toxicity: new insights into protein folding, misfolding diseases and biological evolution. *J. Mol. Med.* 81, 678–699
37. Nekooki-Machida, Y. *et al.* (2009) Distinct conformations of *in vitro* and *in vivo* amyloids of huntingtin-exon1 show different cytotoxicity. *Proc. Natl. Acad. Sci. U. S. A.* 106, 9679–9684
38. Lin, H.K. *et al.* (2017) Fibril polymorphism affects immobilized non-amyloid flanking domains of huntingtin exon1 rather than its polyglutamine core. *Nat. Commun.* 8, 15462
39. Fitzpatrick, A.W.P. *et al.* (2017) Cryo-EM structures of tau filaments from Alzheimer's disease. *Nature* 547, 185–190
40. Guerrero-Ferreira, R. *et al.* (2018) Cryo-EM structure of alpha-synuclein fibrils. *Elife* 7, e36402
41. Iadanza, M.G. *et al.* (2018) The structure of a beta2-microglobulin fibril suggests a molecular basis for its amyloid polymorphism. *Nat. Commun.* 9, 4517
42. Tuttle, M.D. *et al.* (2016) Solid-state NMR structure of a pathogenic fibril of full-length human alpha-synuclein. *Nat. Struct. Mol. Biol.* 23, 409–415
43. Fitzpatrick, A.W.P. and Saibil, H.R. (2019) Cryo-EM of amyloid fibrils and cellular aggregates. *Curr. Opin. Struct. Biol.* 58, 34–42
44. Dawson, T.M. *et al.* (2018) Animal models of neurodegenerative diseases. *Nat. Neurosci.* 21, 1370–1379
45. Barker, R.A. and Bjorklund, A. (2020) Animal models of Parkinson's disease: are they useful or not? *J. Parkinsons Dis.* Published online July 21, 2020. https://doi.org/10.3233/JPD-202200
46. Davies, S.W. *et al.* (1997) Formation of neuronal intranuclear inclusions underlies the neurological dysfunction in mice transgenic for the HD mutation. *Cell* 90, 537–548
47. Miller, J. *et al.* (2010) Quantitative relationships between huntingtin levels, polyglutamine length, inclusion body formation, and neuronal death provide novel insight into Huntington's disease molecular pathogenesis. *J. Neurosci.* 30, 10541–10550
48. Petrasch-Parwez, E. *et al.* (2007) Cellular and subcellular localization of Huntington aggregates in the brain of a rat

transgenic for Huntington disease. *J. Comp. Neurol.* 501, 716–730
49. Qin, Z.-H. *et al.* (2004) Huntingtin bodies sequester vesicle-associated proteins by a polyproline-dependent interaction. *J. Neurosci.* 24, 269–281
50. Waelter, S. *et al.* (2001) Accumulation of mutant huntingtin fragments in aggresome-like inclusion bodies as a result of insufficient protein degradation. *Mol. Biol. Cell* 12, 1393–1407
51. Gilkey, J.C. and Staehelin, L.A. (1986) Advances in ultrarapid freezing for the preservation of cellular ultrastructure. *J. Electron Microsc. Tech.* 3, 177–210
52. Heuser, J. (2002) Whatever happened to the 'microtrabecular concept. *Biol. Cell.* 94, 561–596
53. Dubochet, J. and Sartori Blanc, N. (2001) The cell in absence of aggregation artifacts. *Micron* 32, 91–99
54. Lu, M. *et al.* (2020) Advanced fluorescence imaging of in situ protein aggregation. *Phys. Biol.* 17, 021001
55. Sigal, Y.M. *et al.* (2018) Visualizing and discovering cellular structures with super-resolution microscopy. *Science (New York, N.Y.)* 361, 880–887
56. Schermelleh, L. *et al.* (2019) Super-resolution microscopy demystified. *Nat. Cell Biol.* 21, 72–84
57. Lu, M. *et al.* (2019) Live-cell super-resolution microscopy reveals a primary role for diffusion in polyglutamine-driven aggresome assembly. *J. Biol. Chem.* 294, 257–268
58. Sahl, S.J. *et al.* (2012) Cellular inclusion bodies of mutant huntingtin exon 1 obscure small fibrillar aggregate species. *Sci. Rep.* 2, 895
59. Díaz-Hernández, M. (2004) Biochemical, ultrastructural, and reversibility studies on huntingtin filaments isolated from mouse and human brain. *J. Neurosci.* 24, 9361–9371
60. Peskett, T.R. *et al.* (2018) A liquid to solid phase transition underlying pathological huntingtin exon1 aggregation. *Mol. Cell* 70, 588–601
61. Bäuerlein, F.J.B. *et al.* (2017) In situ architecture and cellular interactions of polyQ inclusions. *Cell* 171, 179–187
62. Sahl, S.J. *et al.* (2016) Delayed emergence of subdiffraction-sized mutant huntingtin fibrils following inclusion body formation. *Q. Rev. Biophys.* 49, e2
63. Li, L. *et al.* (2016) Real-time imaging of Huntingtin aggregates diverting target search and gene transcription. *Elife* 5, e17056
64. Digman, M.A. *et al.* (2008) Mapping the number of molecules and brightness in the laser scanning microscope. *Biophys. J.* 94, 2320–2332
65. Moor, H. (1964) Die gefrier-fixation lebender zellen und ihre anwendung in der elektronenmikroskopie. *Z. Zellforsch. Mikrosk. Anat.* 62, 546–580
66. Moor, H. and Riehle, U. (1968) Snap-freezing under high pressure: a new fixation technique for freeze-etching. In *Proc 4th Eur Reg Conf Electron Microsc* (2), pp. 33–44
67. Riehle, U. and Höchli, M. (1973) The theory and technique of high pressure freezing. In *Freeze-Etching. Techniques and Applications* (Benedetti, E.L. and Favard, P., eds), pp. 31–61, Societe Francais de Microscopie Electronique
68. Li, X. *et al.* (2013) Electron counting and beam-induced motion correction enable near-atomic-resolution single-particle cryo-EM. *Nat. Methods* 10, 584–590
69. Bammes, B.E. *et al.* (2012) Direct electron detection yields cryo-EM reconstructions at resolutions beyond 3/4 Nyquist frequency. *J. Struct. Biol.* 177, 589–601
70. McMullan, G. *et al.* (2009) Detective quantum efficiency of electron area detectors in electron microscopy. *Ultramicroscopy* 109, 1126–1143
71. Rigort, A. and Bäuerlein, F.J.B. *et al.* (2012) Focused ion beam micromachining of eukaryotic cells for cryoelectron tomography. *Proc. Natl. Acad. Sci. U. S. A.* 109, 4449–4454
72. Mahamid, J. *et al.* (2016) Visualizing the molecular sociology at the HeLa cell nuclear periphery. *Science* 351, 969–972
73. Danev, R. *et al.* (2014) Volta potential phase plate for in-focus phase contrast transmission electron microscopy. *Proc. Natl. Acad. Sci. U. S. A.* 111, 15635–15640
74. Danev, R. and Baumeister, W. (2017) Expanding the boundaries of cryo-EM with phase plates. *Curr. Opin. Struct. Biol.* 46, 87–94
75. Beck, M. and Baumeister, W. (2016) Cryo-electron tomography: can it reveal the molecular sociology of cells in atomic detail? *Trends Cell Biol.* 26, 825–837
76. Gruber, A. *et al.* (2018) Molecular and structural architecture of polyQ aggregates in yeast. *Proc. Natl. Acad. Sci. U. S. A.* 115, E3446–E3453
77. Krobitsch, S. and Lindquist, S. (2000) Aggregation of huntingtin in yeast varies with the length of the polyglutamine expansion and the expression of chaperone proteins. *Proc. Natl. Acad. Sci. U. S. A.* 97, 1589–1594
78. Scior, A. *et al.* (2018) Complete suppression of Htt fibrilization and disaggregation of Htt fibrils by a trimeric chaperone complex. *EMBO J.* 37, 282–299
79. Wegmann, S. *et al.* (2010) Human Tau isoforms assemble into ribbon-like fibrils that display polymorphic structure and stability. *J. Biol. Chem.* 285, 27302–27313
80. Ossato, G. *et al.* (2010) A two-step path to inclusion formation of huntingtin peptides revealed by number and brightness analysis. *Biophys. J.* 98, 3078–3085
81. Milanesi, L. *et al.* (2012) Direct three-dimensional visualization of membrane disruption by amyloid fibrils. *Proc. Natl. Acad. Sci. U. S. A.* 109, 20455–20460
82. Guedes-Dias, P. and Holzbaur, E.L.F. (2017) Huntingtin fibrils poke membranes. *Cell* 171, 32–33
83. Dubochet, J. and McDowall, A.w. (1981) Vitrification of pure water for electron microscopy. *J. Microsc.* 124, 3–4
84. Al-Amoudi, A. *et al.* (2005) Cutting artefacts and cutting process in vitreous sections for cryo-electron microscopy. *J. Struct. Biol.* 150, 109–121
85. Hsieh, C-E. *et al.* (2006) Towards high-resolution three-dimensional imaging of native mammalian tissue: electron tomography of frozen-hydrated rat liver sections. *J. Struct. Biol.* 153, 1–13
86. McDowall, A.W. *et al.* (1983) Electron microscopy of frozen hydrated sections of vitreous ice and vitrified biological samples. *J. Microsc.* 131, 1–9
87. Marko, M. *et al.* (2007) Focused-ion-beam thinning of frozen-hydrated biological specimens for cryo-electron microscopy. *Nat. Methods* 4, 215–217
88. Mahamid, J. *et al.* (2015) A focused ion beam milling and lift-out approach for site-specific preparation of frozen-hydrated lamellas from multicellular organisms. *J. Struct. Biol.* 192, 262–269
89. Zachman, M.J. *et al.* (2016) Site-specific preparation of intact solid–liquid interfaces by label-free in situ localization and cryo-focused ion beam lift-out. *Microsc. Microanal.* 22, 1338–1349
90. Schaffer, M. *et al.* (2019) A cryo-FIB lift-out technique enables molecular-resolution cryo-ET within native *Caenorhabditis elegans* tissue. *Nat. Methods* 16, 757–762
91. Guo, Q. *et al.* (2018) In situ structure of neuronal C9orf72 poly-GA aggregates reveals proteasome recruitment. *Cell* 172, 696–705
92. Brady, W.J. *et al.* (2019) Lay responder care for an adult with out-of-hospital cardiac arrest. *N. Engl. J. Med.* 381, 2242–2251
93. Kashiura, M. *et al.* (2017) Association between cardiopulmonary resuscitation duration and one-month neurological outcomes for out-of-hospital cardiac arrest: a prospective cohort study. *BMC Anesthesiol.* 17, 59
94. Nikonenko, A.G. *et al.* (2009) Structural features of ischemic damage in the hippocampus. *Anat. Rec. (Hoboken)* 292, 1914–1921
95. Petito, C.K. and Pulsinelli, W.A. (1984) Sequential development of reversible and irreversible neuronal damage following cerebral ischemia. *J. Neuropathol. Exp. Neurol.* 43, 141–153
96. McGee-Russell, S.M. *et al.* (1970) A combined light and electron microscope study of early anoxic-ischaemic cell change in rat brain. *Brain Res.* 20, 193–200
97. Rahaman, P. and Del Bigio, M.R. (2018) Histology of brain trauma and hypoxia-ischemia. *Acad. Forensic Pathol.* 8, 539–554
98. Shahmoradian, S.H. *et al.* (2019) Lewy pathology in Parkinson's disease consists of crowded organelles and lipid membranes. *Nat. Neurosci.* 22, 1099–1109
99. Lewis, A.J. *et al.* (2019) Imaging of post-mortem human brain tissue using electron and X-ray microscopy. *Curr. Opin. Struct. Biol.* 58, 138–148

100. Takahashi, K. *et al.* (2007) Induction of pluripotent stem cells from adult human fibroblasts by defined factors. *Cell* 131, 861–872
101. Vera, E. and Studer, L. (2015) When rejuvenation is a problem: challenges of modeling late-onset neurodegenerative disease. *Development* 142, 3085–3089
102. Tang, Y. *et al.* (2017) Direct reprogramming rather than iPSC-based reprogramming maintains aging hallmarks in human motor neurons. *Front. Mol. Neurosci.* 10, 359
103. Vierbuchen, T. *et al.* (2010) Direct conversion of fibroblasts to functional neurons by defined factors. *Nature* 463, 1035–1041
104. Oh, Y. (2019) Patient-specific pluripotent stem cell-based Parkinson's disease models showing endogenous alpha-synuclein aggregation. *BMB Rep.* 52, 349–359
105. Miller, J.D. *et al.* (2013) Human iPSC-based modeling of late-onset disease via progerin-induced aging. *Cell Stem Cell* 13, 691–705
106. Victor, M.B. *et al.* (2018) Striatal neurons directly converted from Huntington's disease patient fibroblasts recapitulate age-associated disease phenotypes. *Nat. Neurosci.* 21, 341–352
107. Strtohl, F. and Kaminski, C.F. (2016) Frontiers in structured illumination microscopy. *Optica* 3, 667–677
108. Moerner, W.E. (2012) Microscopy beyond the diffraction limit using actively controlled single molecules. *J. Microsc.* 246, 213–220
109. Huang, F. *et al.* (2013) Video-rate nanoscopy using sCMOS camera-specific single-molecule localization algorithms. *Nat. Methods* 10, 653–658
110. Jones, S.A. *et al.* (2011) Fast, three-dimensional super-resolution imaging of live cells. *Nat. Methods* 8, 499–508
111. Hell, S.W. and Wichmann, J. (1994) Breaking the diffraction resolution limit by stimulated emission: stimulated-emission-depletion fluorescence microscopy. *Opt. Lett.* 19, 780–782
112. Klar, T.A. *et al.* (2001) Breaking Abbe's diffraction resolution limit in fluorescence microscopy with stimulated emission depletion beams of various shapes. *Phys. Rev. E* 64, 066613
113. Baumeister, W. (2005) A voyage to the inner space of cells. *Protein Sci.* 14, 257–269
114. Plitzko, J.M. *et al.* (2009) Correlative cryo-light microscopy and cryo-electron tomography: from cellular territories to molecular landscapes. *Curr. Opin. Biotechnol.* 20, 83–89
115. Arnold, J. *et al.* (2016) Site-specific cryo-focused ion beam sample preparation guided by 3D correlative microscopy. *Biophys. J.* 110, 860–869
116. Moser, F. *et al.* (2019) Cryo-SOFI enabling low-dose super-resolution correlative light and electron cryo-microscopy. *Proc. Natl. Acad. Sci. U. S. A.* 116, 4804–4809
117. Bartesaghi, A. and Subramaniam, S. (2009) Membrane protein structure determination using cryo-electron tomography and 3D image averaging. *Curr. Opin. Struct. Biol.* 19, 402–407
118. Förster, F. and Hegerl, R. (2007) Structure determination in situ by averaging of tomograms. *Methods Cell Biol.* 79, 741–767
119. Shahmoradian, S.H. *et al.* (2017) Three-dimensional imaging of biological tissue by cryo X-ray ptychography. *Sci. Rep.* 7, 6291
120. Chichon, F.J. *et al.* (2012) Cryo X-ray nano-tomography of vaccinia virus infected cells. *J. Struct. Biol.* 177, 202–211
121. Theillet, F.X. *et al.* (2016) Structural disorder of monomeric alpha-synuclein persists in mammalian cells. *Nature* 530, 45–50
122. Miao, K. and Wei, L. (2020) Live-cell imaging and quantification of polyQ aggregates by stimulated Raman scattering of selective deuterium labeling. *ACS Cent. Sci.* 6, 478–486
123. Hoffman, D.P. *et al.* (2020) Correlative three-dimensional super-resolution and block-face electron microscopy of whole vitreously frozen cells. *Science* 367, eaaz5357
124. M'Saad, O. and Bewersdorf, J. (2020) Light microscopy of proteins in their ultrastructural context. *Nat. Commun.* 11, 3850
125. Trinkaus, V.A. *et al.* (2020) *In situ* architecture of neuronal α-Synuclein inclusions. *bioRxiv* Posted online August 20, 2020. https://doi.org/10.1101/2020.08.07.234138
126. Schaefer, T. *et al.* (2019) Amyloid-like aggregates cause lysosomal defects in neurons via gain-of-function toxicity. *bioRxiv* Posted online August 20, 2020 https://doi.org/10.1101/2019.12.16.877431